

AUTONOMOUS NAVIGATION AND SAMPLE COLLECTION FOR THE LOW-COST MAIN-BELT ASTEROID SAMPLE RETURN MISSION

Alexander SUKHANOV

*Space Research Institute (IKI) of Russian Academy of Sciences
117997, 84/32 Profsoyuznaya Str., Moscow, Russia
sukhanov@iki.rssi.ru*

Otávio DURÃO

*National Institute for Space Researches (INPE)
1758 Av. Dos Astronauticas, São José dos Campos, SP – Brazil
duraod@dem.inpe.br*

ABSTRACT – *A main-belt asteroid sample return without landing on the asteroid is considered: the spacecraft collects the sample during the asteroid flyby, crossing the dust cloud produced by a projectile, and delivers the sample to the Earth. The paper discusses the spacecraft navigation, the projectile targeting, and the sample ejection. A way of autonomous navigation providing close approach to the asteroid is suggested. The sample ejection is considered for two projectile types: passive, using only the impact energy; and active, carrying an explosive inside. The mass of the sample to be collected is estimated. Other possible ways of the spacecraft navigation and projectile targeting are also considered.*

KEYWORDS: asteroids, sample return, autonomous navigation, projectile, sample collection.

NOMENCLATURE

D	the projectile miss of the nominal impact point in B-plane, km
E	impact energy, MJ = kg·(km/s) ²
h	distance between the projectile impact point and the spacecraft path, km (see Fig. 3)
m	the projectile mass, kg
M	ejected mass, kg
m_e	the explosive mass, kg
r	current distance from the impact point to the spacecraft, km
R	maximum particle distance from the impact at time τ , $R = U\tau$, km
S	area of the sample collector, m ²
t_s	time between the projectile separation and the closest approach, s
u	ejection velocity, km/s
U	maximum ejection velocity, km/s
v	spacecraft flyby velocity, km/s
V	ejecta volume, km ³
x	spacecraft position in the flyby trajectory counted from the closest approach to the impact, km (see Fig. 5)

δd	the uncertainty in the asteroid flyby distance, determined before the projectile separation, km
δh	the uncertainty in the distance h stipulated by $\delta\sigma$, km
$\delta\sigma$	the projectile angular separation error, degree
Δv	the projectile separation velocity, m/s
$\Delta v_t, \Delta v_n$	tangent and normal components of the separation velocity, m/s
η	the impact or explosive effectiveness
λ	a constant, km/s/kg
μ	collected sample mass, mg
σ	projectile separation angle, $\sigma = \arctan(\Delta v_n/\Delta v_t)$, degree
τ	time between the impact and the spacecraft closest approach to the impact point (the spacecraft delay time, see Fig. 3), s
$\varphi_1, \varphi_2, \psi$	angles defined in Figs. 4, 5, degree
χ	specific energy of the explosive, MJ/kg

INTRODUCTION

A main-belt asteroid sample return mission without landing on the asteroid was considered in [1]. The mission concept is similar to the one suggested for the Aladdin Phobos and Deimos sample return mission and to the one that was also independently considered for another Phobos sample return mission [2]. The mission concept considered in [1] is the following: 1) the spacecraft is launched into a trajectory that performs a rendezvous with the asteroid and returns to the Earth; 2) before the encounter a projectile is separated from the spacecraft, hits the asteroid and produces a dust cloud; 3) the spacecraft crosses the cloud and picks up the dust particles into a collector; 4) the collected samples are placed into a recoverable capsule which is detached from the spacecraft before reentry into the Earth's atmosphere. It was also suggested to use Venus and Earth Gravity Assistance (VEGA) maneuver in order to lower the launch energy. A numerous mission opportunities were considered in details in [1] for the launch in 2004–2010. Apart from the sample collection of the primary targets, a few more asteroids can be also encountered as secondary targets in some of the mission opportunities considered in [1].

The main problems in such mission are the spacecraft navigation providing a close approach to the asteroid, the projectile accurate targeting, and the sample collection. Possible solutions of the problems also were considered in [1]. This paper gives an extended analysis of the spacecraft autonomous navigation and the projectile targeting.

SPACECRAFT NAVIGATION

The spacecraft motion relative to the encountered asteroid is approximately uniform and rectilinear, in the vicinity of the closest approach. For instance, the difference in the spacecraft relative velocity near the closest approach, as well as in the previous ten days, does not exceed 40 m/s and 0.15 deg in the velocity value and direction respectively, for any mission option. Therefore, we can assume that the spacecraft relative velocity is constant in the vicinity of the closest approach; this assumption simplifies the subsequent analysis.

To fulfill the mission goal, the spacecraft has to approach the asteroid very closely. This very close approach is only possible using an autonomous optical navigation. All the primary targets considered in [1] are bright and the onboard observations of the asteroids can begin quite long before the closest approach if sensitivity of the spacecraft camera is higher than 8 stellar magnitude.

DS1 has proven [3] that the autonomous navigation can lower the uncertainty of the relative spacecraft-to-asteroid position down to 3 km in B-plane and allow the spacecraft to approach the asteroid to the distance of 15 km. However, a smaller relative position uncertainty and a closer approach to the asteroid may be necessary for the sample return mission. The autonomous navigation system similar to DS1 can

provide the crosstrack error in the mutual spacecraft and asteroid position down to 0.5 km in 6 hours before the closest approach [4]. However, this error holds true only for a small asteroid because of the asteroid centroiding problem. The problem appears due to the not full illumination phase of the asteroids as is seen from the approaching spacecraft and possible irregular asteroid shape. Assuming that the asteroid can be centroided with an error of 1% of its diameter (which is quite optimistic) we obtain the error of about 5 km for 2 Pallas and 4 Vesta, about 2 km for 16 Psyche, and more than 1 km for several other mission options in [1]. There is another serious problem of the spacecraft and projectile targeting: the asteroid of an uncertain, irregular shape can put its elongated part in the spacecraft path during the closest approach which will lead to the spacecraft collision with the asteroid (see Fig. 1a). Or, vice versa, the asteroid can turn by its short side at the projectile approach time and the projectile will miss the asteroid (see Fig. 1b).

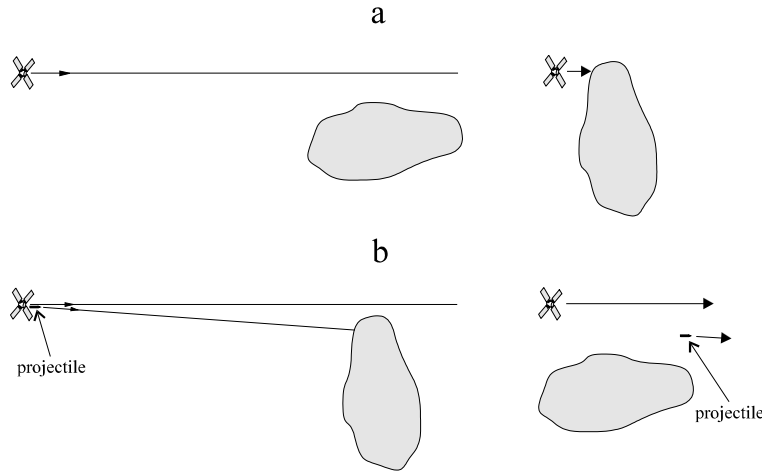


Fig. 1. Possible Problems with an Elongated Asteroid

Considering one possible solution of the problems in details. It is to use for the navigation only, the asteroid images obtained exactly at times equal to integer numbers of the asteroid rotation period. In this case the asteroid will be in the same attitude at the closest approach, as it will have been seen in the images used for the spacecraft and projectile targeting (see Fig. 2).

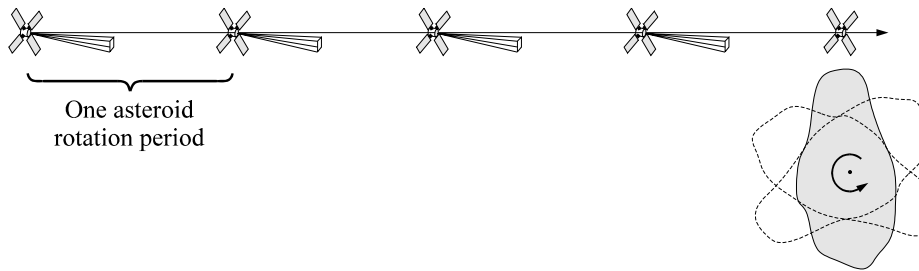


Fig. 2. The Autonomous Navigation Using Images Obtained at Times Multiple to the Asteroid Rotation Period

The asteroid centroiding also is not needed in this case: the spacecraft motion can be determined with respect to the asteroid illuminated limb. The rotation periods are known quite accurately for many main-belt asteroids [5, 6]. Taking the following assumptions: i) The onboard observations of the asteroid begin ten days and end one asteroid rotation period before the closest approach. ii) The reference star positions in the onboard catalogue are accurate to 1 arc sec ($5 \mu\text{rad}$). iii) Angular resolution of the spacecraft camera is 2 arc sec ($10 \mu\text{rad}$; the DS1 MICAS camera resolution was $13 \mu\text{rad}$ [7], although initial requirement was $5 \mu\text{rad}$ [4]). Then the asteroid and star positions in the camera image can be measured

with errors within 1 arc sec. Assuming that the errors in the same image are independent, and taking into account also the independent errors of the reference star catalogue, obtain that the asteroid angular position can be measured with accuracy of about $\sqrt{3} \approx 1.7$ arc sec (8.4 μ rad). iv) The errors of different observations separated by one or more asteroid rotation periods are independent.

The proposed navigation method gives an error in the B-plane within 1.5 km one asteroid rotation period before the closest approach for the following targets: 4 Vesta (error 0.8 km), 16 Psyche (0.5 km), 40 Harmonia (1.5 km), 55 Pandora (0.8 km), 115 Thyra (1.2 km), 250 Bettina (1.0 km), 317 Roxane (1.4 km). For all other asteroids with known rotation periods the errors are between 1.6 and 8 km. Thus, this simple and elegant solution provides quite good accuracy of the spacecraft-to-asteroid position in the B-plane for a few mission options.

Note that the time of the closest approach carry an error, which, nevertheless, will not influence the suggested method significantly. The procedure assumes an uncertainty in the relative spacecraft and asteroid position equal to 300 km along the spacecraft path. Then, as can be easily calculated from the asteroid rotation period and the spacecraft flyby velocity, the error in the asteroid attitude will be of about 1.5 deg for Psyche and less than 1 deg for other asteroids. This error cannot noticeably change the asteroid cross-section orthogonal to the spacecraft path.

The rotation periods of some of the asteroids contain rather big error [5, 6]. However, the knowledge of the rotation periods can be improved, before the mission, using more asteroid observations.

PROJECTILE TARGETING

The projectile targeting is illustrated by Fig. 3. Assuming $t_s > 0$, $\tau > 0$ and $t_s \gg \tau$, the ejected particles will have widely varying velocities after the impact. However, considering a typical ejection velocity u provides $\tau \approx h/u$.

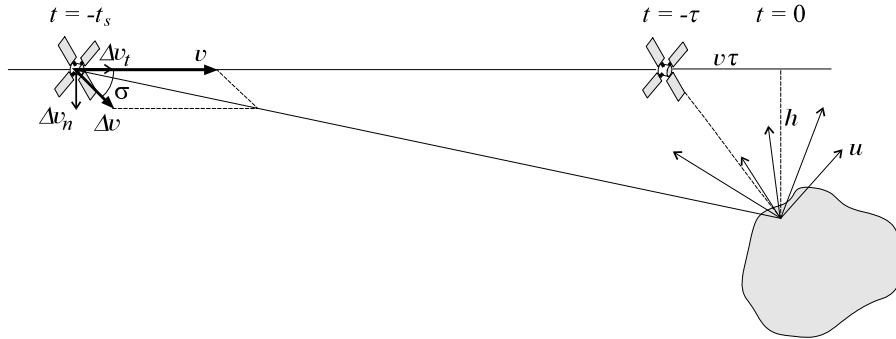


Fig. 3. Projectile Targeting

The necessary condition for the ejection of a considerable amount of the sample using the impact energy is

$$u \ll v \quad (1)$$

The sample ejection velocities and the delay time τ are considered in more details in the next section of the paper. In the framework of the considered uniform linear motion model

$$\Delta v_n = \frac{h}{t_s}, \quad \Delta v_t = v \frac{\tau}{t_s} \quad (2)$$

Then

$$\tan \sigma = \frac{\Delta v_n}{\Delta v_t} = \frac{h}{v\tau} \approx \frac{u}{v} \ll 1 \quad (3)$$

Thus, the separation angle is small and does not depend upon the separation time and flyby distance and

$$\Delta v = \sqrt{\Delta v_t^2 + \Delta v_n^2} \approx \Delta v_t \quad (4)$$

Considering the projectile angular separation error $\delta\sigma$. The uncertainty in the distance h stipulated by the error is

$$\delta h = \Delta v_n t_s \delta\sigma = v\tau \delta\sigma \approx \frac{v}{u} h \delta\sigma \quad (5)$$

Thus, the uncertainty also does not depend on the separation time and flyby distance. Since the uncertainty and the projectile separation error are independent, the projectile miss (D) of the nominal impact point in the B-plane is

$$D = \sqrt{\delta d^2 + \delta h^2} \quad (6)$$

The miss distance is very important for the projectile targeting because it determines the maximum limit for the distance of the targeting point to the asteroid local horizon. Error in the separation velocity value only influences the delay time τ and is not as important.

THE SAMPLE EJECTION

Inert Projectile

In this case a projectile produces the asteroid sample ejection by means of the impact energy. Since the impact velocity is nearly equal to the spacecraft flyby velocity v , then the impact energy is

$$E = \frac{mv^2}{2} \quad (7)$$

where m is the projectile mass. Specific impact energy is quite high for the mission options considered above, it varies from 8.4 to 103 MJ per 1 kg of the projectile mass. However only part ηE of the energy can be transformed into the ejection, where η is the impact effectiveness. The effectiveness is low because a significant part of the impact energy is transformed into heating. Perhaps it is reasonable to drop a cluster of projectiles (as it was proposed for the Aladdin mission) covering an area under the spacecraft path. This cluster of projectiles can raise the mission reliability because a single projectile hitting a rock can produce an aside ejection, not crossing the spacecraft flyby trajectory. Also several projectiles being separated with slightly different separation angles can compensate the uncertainty in Equation 5 due to the separation error.

Exploding Projectile

Considering a projectile containing an explosive inside, the explosion energy is

$$E = \chi m_e \quad (8)$$

The highest value for χ (1.4 MJ/kg) are found for the explosives hexogen (RDX) and octogen (HMX) [8]. This energy is much lower than the projectile impact energy. However, using explosive have a few

advantages, such as the following. First, a pencil-like shaped projectile can penetrate the asteroid to some depth and then the explosion will provide samples from deeper layers. Second, the effectiveness η of the explosion probably can be higher than the one with the impact. Third, perhaps it is possible to direct the explosion upward somehow, thus raising spatial density of the dust cloud in the spacecraft way. It is also possible to increase the transferred energy by using both the impact energy and the explosion for the ejection.

Ejection Model

Assuming that the asteroid particles are ejected with velocities u uniformly distributed between 0 and U , i.e. the ejected mass having velocity u is

$$dM = \lambda du$$

where λ is a constant. Since the entire ejected mass is

$$M = \int_0^M dM = \lambda \int_0^U du = \lambda U,$$

it follows that

$$dM = \frac{M}{U} du \quad (9)$$

The effective energy transformed into the ejection of the mass M is

$$\eta E = \frac{1}{2} \int_0^M u^2 dM = \frac{M}{2U} \int_0^U u^2 du = \frac{MU^2}{6}$$

Thus,

$$M = \frac{6\eta E}{U^2} \quad (10)$$

The model assumes that the projectile impact or explosion energy, transformed into the sample ejection, dissipates uniformly between two circular conical sectors with axis colinear to the projectile velocity and apex angles φ_1 and φ_2 respectively, and sector angle ψ (see Fig. 4).

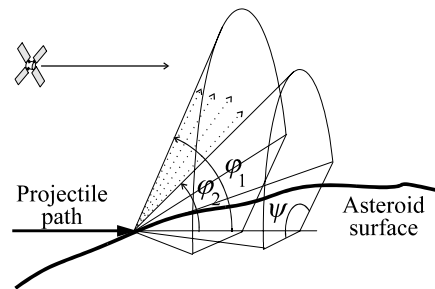


Fig. 4. Sample Ejection Model

This model is quite general because varying the angles it provides different shapes of the ejected cloud. Gravitational acceleration near the asteroids is small (within 0.25 m/s^2 for the options considered in [1]).

Therefore it is possible to neglect the ejection velocity change during few tens of seconds if the velocity is in the order of 100 m/s. Then, the volume of the dust cloud in time τ after the impact will be $V = \psi c R^3 / 3$ where $R = U\tau$ is the maximum particle distance from the impact, $c = \cos\varphi_1 - \cos\varphi_2$. Elementary volume at the distance $r = u\tau \leq R$ from the impact is

$$dV = \psi c r^2 dr$$

Equation (9) gives

$$dM = \frac{M}{R} dr$$

The spatial density of the dust cloud at the distance r from the impact, using Equation (10), can be found as

$$\rho = \frac{dM}{dV} = \frac{M}{\psi c r^2 R} = \frac{6\eta E}{\psi c r^2 R U^2} \quad (11)$$

Sample Collection

Due to the condition (1) it is assumed that the ejected dust cloud is not changed during the time of its crossing by the spacecraft. Now the mass μ of the collected sample can be estimated as follows:

$$\mu = S \int_{x_1}^{x_0} \rho dx$$

where S is area of the sample collector, x is the spacecraft position in the flyby trajectory counted from the closest approach to the impact, $x = h \cot \varphi$ (see Fig. 5).

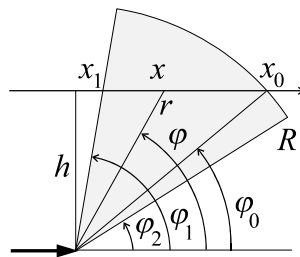


Fig. 5. Crossing the Dust Cloud

Taking into account Equation (11) and relations $r = h/\sin \varphi$, $R = h/\sin \varphi_0$, then

$$\mu = \frac{6\eta ES}{\psi c h R U^2} \int_{\varphi_0}^{\varphi_1} d\varphi = \frac{6\eta ES}{\psi c h^2 U^2} \left(\frac{1}{\sin \varphi_1} - \frac{1}{\sin \varphi_0} \right) \quad (12)$$

Note that in a particular case angle φ_0 can be equal to φ_2 . It is assumed that the parameters U , φ_1 , φ_2 are a priori known; they can be estimated theoretically or by means of ground experiments if there is a guess about the asteroid soil hardness and cohesion. It is assumed that

$$\varphi_2 \leq \varphi_1, \quad \varphi_2 \leq \pi - \varphi_1 \quad (13)$$

Then an optimal value of the φ_0 angle providing maximum in Equation (12) can be easily found. Note that the necessary condition of $\max_{\varphi_0} \left\{ \varphi_1 - \varphi_0 \right\} \sin \varphi_0$ is the equation

$$\varphi_0 + \tan \varphi_0 = \varphi_1 \quad (14)$$

As is seen from Eq. (14), $\varphi_0 < \varphi_1/2$, the optimal value of φ_0 versus φ_1 angle is given in Fig. 6.

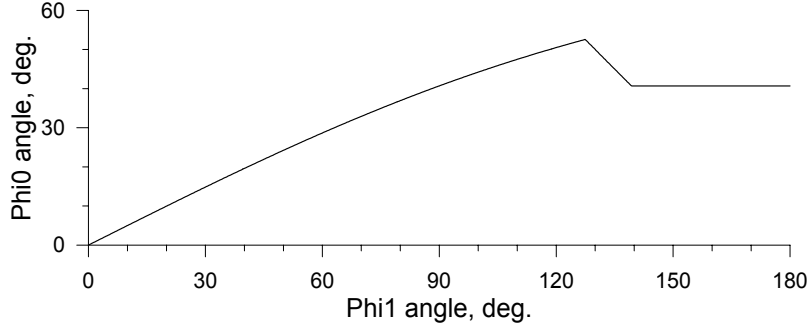


Fig. 6. Optimal φ_0 Angle Versus φ_1 Angle

There are four different cases illustrated by Fig. 7: i) $0 < \varphi_1 < 127.43$ deg and $\varphi_2 \geq \varphi_0$ where φ_0 is defined by Fig. 6, then optimal $\varphi_0 = \varphi_2$ (Fig. 7a); ii) $0 < \varphi_1 < 127.43$ deg and $\varphi_2 < \varphi_0$ where φ_0 is defined by Fig. 6, then optimal φ_0 is given by the ascending curve in Fig. 6 (Fig. 7b); iii) 127.43 deg $\leq \varphi_1 < 139.29$ deg, then optimal $\varphi_0 = 180$ deg $- \varphi_1$ (Fig. 7c); iv) 139.29 deg $\leq \varphi_1 < 180$ deg, then optimal $\varphi_0 = 40.71$ deg (Fig. 7d).

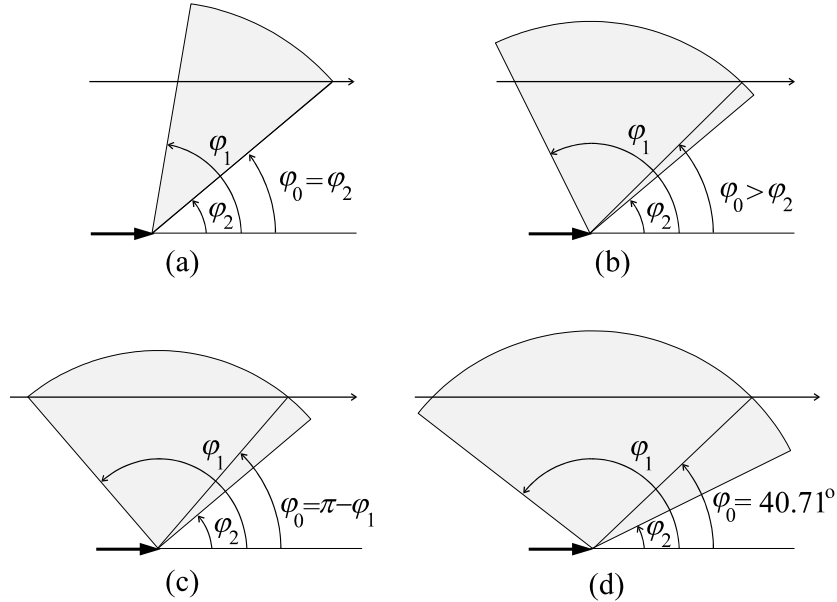


Fig. 7. Different Cases of the Optimal Crossing the Dust Cloud

It is interesting to note that the parameters E , η , ψ , h do not influence the optimal flyby configuration. Note that the second constraint of Eq. (13) is empirical and means that the ejection resultant cannot be directed backward with respect to the projectile motion. However all results given above can be easily

generalized for the case $\varphi_2 > \pi - \varphi_1$. After the φ_0 angle value is found, the delay time τ can be calculated as follows:

$$\tau = \frac{R}{U} = \frac{h}{U \sin \varphi_0} \quad (15)$$

Considering the particular case when $90 \text{ deg} < \varphi_1 \leq 139.29 \text{ deg}$, $\varphi_2 = 180 \text{ deg} - \varphi_1$, and $\psi = 180 \text{ deg}$, which corresponds, for example, to an explosion in all directions orthogonal to the projectile longitudinal axis ejecting the asteroid soil in upper hemisphere. In this case $\varphi_0 = \varphi_2$ and Equation (12) gives

$$\mu = \frac{3\eta ES}{\pi h^2 U^2} \beta - 2\varphi_2 \gamma \tan \varphi_2 \quad (16)$$

Note that the Equations (12) and (16) are very approximate because of inevitable uncertainties in the h , η , U , φ_1 , φ_2 , ψ parameters and the assumption about the uniform distribution of the ejection velocities. Neither of these expressions can be used directly for the spacecraft targeting. For instance, due to a possible error in h value, it is reasonable to increase a little the delay time τ in order not to miss the dust cloud. This delay time increase will lead to a lower spatial density of the crossed dust cloud and higher projectile separation velocity in the value $\Delta v/\tau$, where $\Delta \tau$ is the delay time increment. Nevertheless, the results obtained allow one estimation of the collectable sample amount; in addition, the delay time τ and projectile separation velocity Δv can be estimated from Equations (2), (4) and (15).

NUMERICAL EXAMPLE

Considering the 16 Psyche sample return mission to be launched in 2004. This option is quite good because the asteroid itself is of a certain interest, the launch C_3 ($8.84 \text{ km}^2/\text{s}^2$) and flyby velocity (4.53 km/s) are very low comparing with other options, and there are three possible secondary targets [1]. However, the launch date for this option is too close in the future.

The example assumes that the onboard observations of the asteroid begin 10 days before the closest approach (CA). At that time the spacecraft will be at $3.9 \times 10^6 \text{ km}$ from Psyche, the asteroid angular diameter will be about 14 arc sec ($67 \text{ } \mu\text{rad}$), its brightness will be of 1.5 magnitude. Considering the navigation method described in the section "Spacecraft Navigation", the autonomous navigation uses only images made in the times multiple of the asteroid rotation period (which equals to 4.196 hr for Psyche [5, 6, 9]). The example also assumes that the maximum observation error in inertial space is 1.73 arc sec ($8.4 \text{ } \mu\text{rad}$), and that the uncertainties in the spacecraft position and velocity with respect to the asteroid due to the ground observations are 300 km and 1 m/s respectively. Fig. 8 gives the maximum error of the flyby altitude determination by means of the onboard observations versus observation time.

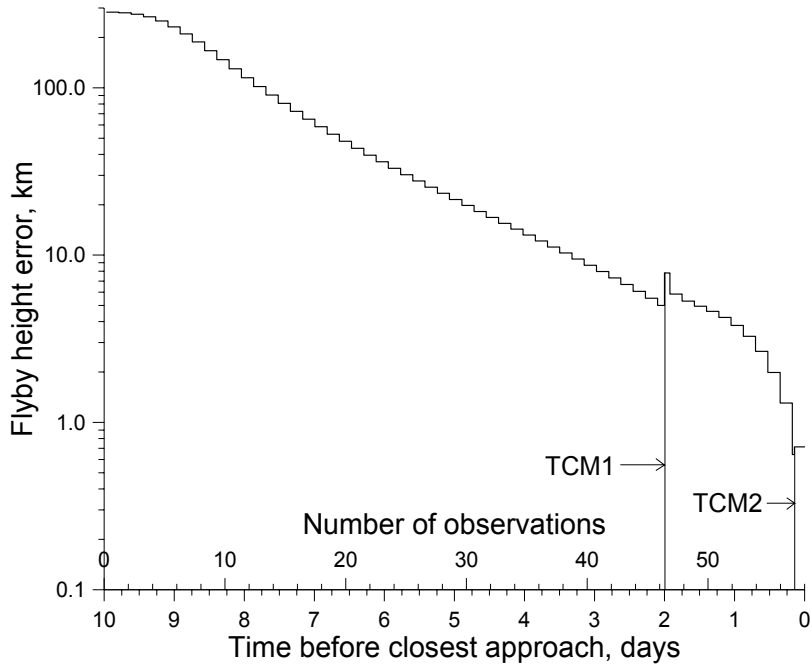


Fig. 8. Error of the flyby altitude determination for 16 Psyche asteroid

Two days before CA (after the 46th observation, when the error is 5 km, see Fig. 8) the example supposes that the first trajectory correction maneuver (TCM1) is performed, targeting the spacecraft in about 10 km above the asteroid limb. The flyby altitude uncertainty defines the error to be corrected by the maneuver, due to the ground observations, assuming that the error is maximum, i.e. equal to 300 km. In this case the TCM1 value is about 1.7 m/s. As is seen in Fig. 8, the maneuver deteriorates the altitude determination accuracy due to an error in the maneuver execution. The calculation assumes that the error is random and equal to 2 percent of the maneuver value in any direction. The last, 57th, onboard observation is made 4.196 hours before CA. About 40 minutes after this observation (3.5 hours before CA) the second trajectory correction maneuver (TCM2) is carried out targeting the spacecraft 3 km above the asteroid limb. Assuming that TCM2 corrects 15-km offset in B-plane (7-km difference between the first and second targeting plus 7.8-km error after TCM1, see Fig. 8), then TCM2 is about 1.2 m/s. The final flyby altitude error δd , taking into account TCM2 execution error, is about 0.7 km (see Fig. 8). This error is larger than the one mentioned in the section “Spacecraft Navigation” (0.5 km) because errors of the correction maneuver executions were not taken into account in that section. However, it should be noted that the example considers worst cases, when both TCM1 and TCM2 have maximum values. The 2% execution value is also rather pessimistic. Therefore, it can be expected that the real Psyche flyby altitude uncertainty δd will be between 0.5 and 0.7 km.

The example is for a projectile separation 30 minutes after TCM2 (i.e. 3 hours before CA) targeted 2 km below the asteroid local horizon. Thus, the nominal value of the h distance is 5 km. The separation angular error $\delta\sigma$ is assumed equal to 20 arc min (we admit that this value is quite optimistic). Supposing a sample collector area $S = 0.5 \text{ m}^2$ (that is much bigger than the 0.1 m^2 Stardust spacecraft collector [10]).

Assuming several 1-kg inert projectiles separated from the spacecraft and that a successful impact produces an ejection with efficiency $\eta = 0.1$ and ejection angles $\varphi_1 = 90 \text{ deg}$, $\varphi_2 = 45 \text{ deg}$, $\psi = 120 \text{ deg}$ (see Fig. 3), and a maximum ejection velocity $U = 200 \text{ m/s}$, then the values of the parameters of the projectiles separation, impact, and the sample collection are the following: $\Delta v = 14.8 \text{ m/s}$, $\sigma = 1.8 \text{ deg}$, $\delta h = 0.9 \text{ km}$, $D = 1.2 \text{ km}$, $\tau = 35 \text{ s}$, $\varphi_0 = 45 \text{ deg}$, $\mu = 1.2 \text{ mg}$ for each successful impact.

Assuming that the projectile mass is 10 kg and the explosive mass is 5 kg, the explosion efficiency $\eta = 0.3$, the maximum ejection velocity is $U = 500$ m/s, the ejection angles are $\varphi_1 = 120$ deg, $\varphi_2 = 60$ deg, $\psi = 120$ deg. Then $\Delta v = 4.9$ m/s, $\sigma = 5.5$ deg, $\delta h = 0.3$ km, $D = 0.8$ km, $\tau = 12$ s, $\varphi_0 = 60$ deg, $\mu = 0.2$ mg.

Thus, for the considered example the maximum collected mass can be of order of 0.1 to 1 mg. Note that the goal of Stardust mission is to recover more than one thousand comet dust particles larger than 15 microns in diameter; the mass of this amount is of order of 0.01 mg.

Note that the demands to the projectile targeting accuracy can be lowered if the projectile separation time is closer to the impact time. The short time between these two events also will give more time for the orbit determination and projectile targeting. However, in this case the projectile separation velocity will increase. As is seen in the numerical example, this increment is quite possible for the case of the projectile explosion with the considered parameters, for which the separation velocity is low. Note that if the projectile separation mechanism is available, perhaps it is reasonable to calculate the separation time assuming the separation velocity as large as the mechanism permits.

OTHER POSSIBLE WAYS OF NAVIGATION

Below a few more possible ways of providing the spacecraft close approach to the asteroid and the projectile accurate targeting will be considered in less details.

Use of a Small Asteroid

A simplest way to avoid the problems of the asteroid centroiding or of the elongated asteroid (see Spacecraft Navigation section) is the use of a small asteroid of 5–10 km in diameter for the sample return mission. As it was proven in Deep Space 1 mission a very close approach to such asteroid is possible. However, the sample return of a small asteroid may be of low interest for science.

Use of the Asteroid Shape and Rotation Data

Another way of providing the spacecraft accurate navigation is the use of the asteroid shape and rotation data in the autonomous navigation. The data being put into the onboard computer can provide an accurate prediction of the spacecraft and projectile motion with respect to the asteroid local horizon. The asteroid rotation and shape data can be obtained by means of both the ground-based observations and onboard ones.

As mentioned before accurate rotation data were obtained for many asteroids by means of ground observations [5, 6]. The most informative ground observations for the asteroid shape determination are occultations: by observing star occultation by an asteroid from different points on the Earth [11, 12]. However occultations are quite rare events and allow to obtain an approximate shape of just one section of the asteroid. The asteroid shape data can be improved by means of the observations from the spacecraft itself, although existing CCD cameras do not provide the image quality sufficient for this purpose. Future CCD camera developments may decrease this restriction

Maneuvering Projectile

A more technically complex solution yet is to consider a maneuvering projectile. The projectile can be controlled by the main spacecraft in the following way. The onboard computer determines the projectile angular position with respect to the asteroid horizon using observations by the onboard camera. Then the spacecraft sends a command to the projectile to perform a correction maneuver. This would allow a significant decrease in the projectile miss (6). The projectile can be separated earlier with respectively lower separation velocity and, thus, a higher angular separation error can occur.

Let us consider a spin-stabilized projectile propelled by a pressurized cold gas and controlled by the spacecraft (see Fig. 9).

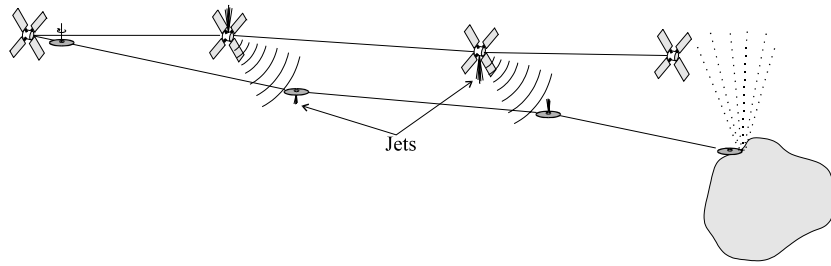


Fig. 9. Active Spacecraft and Projectile Targeting until the Impact

Assuming the spin axis orthogonal to the asteroid local horizon and the cold gas nozzles directed along the axis in two opposite directions. Let us consider 16 Psyche sample return with the same navigation and flyby parameters as in the numerical example given in the previous section. Let us assume that the projectile is separated a day before the closest approach with a two-degree angular separation error $\delta\sigma$. Assuming inert projectile with the same ejection parameters as in the numerical example given in the previous section, we have $\Delta v = 1.72$ m/s, $\sigma = 1.8$ deg, $\tau = 35$ s. Fig. 8 and Eq. (5) give respectively $\delta d = 3.6$ km and $\delta h = 5.5$ km. Thus, the projectile miss (6) is $D = 6.6$ km. Supposing the board camera observation error equal to 1.7 arc sec (see “Spacecraft Navigation” section), the projectile angular separation error can be determined quite accurately by means of the onboard observations of the projectile. If the autonomous navigation described in details in the “Spacecraft Navigation” section is used then the highest accuracy $\delta d = 0.7$ km is reached 4.196 hours before the closest approach (see Fig. 8). Let us assume that the projectile maneuver is performed 3 hours before the closest approach and the maneuver execution error is 5% of the maneuver value. Then the maneuver delta-V is equal to 0.6 m/s and the miss caused by the maneuver execution error is 0.33 km. Assuming the maneuver execution error and the spacecraft navigation error are independent, then the projectile miss is 0.8 km. Note that if the maneuver execution error is bigger than 5% (it can reach 10% for the cold gas without calibration) then a second projectile correction maneuver may be necessary. Thus, the maneuvering projectile can allow much lower separation velocity and much higher angular separation error than the ballistic projectile at the same time providing more accurate projectile targeting.

The projectile can also be designed as a small autonomous spacecraft targeting itself to the asteroid. This solution is similar to the one of the Deep Impact mission. In every case a secondary target encountered prior to the primary one can be used for the navigation testing

ACKNOWLEDGMENTS

The authors are grateful to L. O. Ferreira and D. B. Netto, from INPE, for extremely useful discussions and invaluable information about properties of explosions and hyper-velocity impacts. Also acknowledgements go to J. E. Riedel, from JPL, for precious electronic discussions about imaging navigation for the spacecraft.

REFERENCES

- [1] A. A. Sukhanov, O. Duraõ, D. Lazzaro, “Low Cost Main-Belt Asteroid Sample Return ”; *Journal of Spacecrafts and Rockets*; vol. 38; no. 5; pp 736-744; Sept./Oct. 2001.
- [2] N. A. Eismont, A. A. Sukhanov, “Low Cost Phobos Sample Return Mission,” *ESA/ESOC, Proceedings of the 12th Symposium On Space Flight Dynamics*, Darmstadt, Germany, 2–6 June 1997, pp. 365-370.
- [3] M. A. Dornheim, “DS1 Asteroid Flyby Yields Uncertain Results”, *Aviation Week & Space Technology*, August 2, 1999, p. 32.

- [4] J. E. Riedel, S. Bhaskaran, S. P. Synnott et al., "Navigation for the New Millennium: Autonomous Navigation for Deep Space 1," ESA/ESOC, *Proceedings of the 12th International Symposium on Space Flight Dynamics*, Darmstadt, Germany, 2–6 June 1997, pp. 303–320.
- [5] C.-I. Lagerkvist, "Rotation Periods of Asteroids. Version VIII" [on line], URL http://www.astro.uu.se/planet/rotast_eng.html, August 28, 1996.
- [6] P. Magnusson, "Files in SBN Data Set EAR-A-5-DDR-ASTEROID-SPIN-VECTORS-V4.0 (SPIN)" [on line], URL <http://pdssbn.astro.umd.edu/SBNast/holdings/EAR-A-5-DDR-ASTEROID-SPIN-VECTORS-V4.0.html>, December 29, 1995.
- [7] M. D. Rayman, P. Varghese, D. H. Lehman, L. L. Livesay, "Results from the Deep Space 1 Technology Validation Mission", *Paper IAA-99-IAA.11.2.01 at 50th International Astronautical Congress*, Amsterdam, The Netherlands, 4–8 October, 1999.
- [8] R. Meyer, "Explosives", 3rd ed., VCH Verlagsgesellschaft, FRG, 1987 (USA and Canada: VCH Publishers, New York, USA), p. 71.
- [9] X.-H. Zhou, X.-Y. Yang, "The Rotation of Asteroid (16) Psyche," *Chinese Astronomy and Astrophysics*, No. 6, 1982, pp.57–59.
- [10] "Stardust: Sample Return Capsule and Collector Grid" [on line], URL <http://stardust.jpl.nasa.gov/mission/capsule.html>, Last Updated: July 16, 2001
- [11] International Occultation Timing Association, Inc. (IOTA) [on line], URL <http://www.occultations.org/>, Site last updated on 2001 October 5.
- [12] Dunham, D. W., Planetary Occultations for 1999, *Sky & Telescope*, Vol. 97, No. 2, 1999, pp. 106–109.